

Nanoscale

Accepted Manuscript



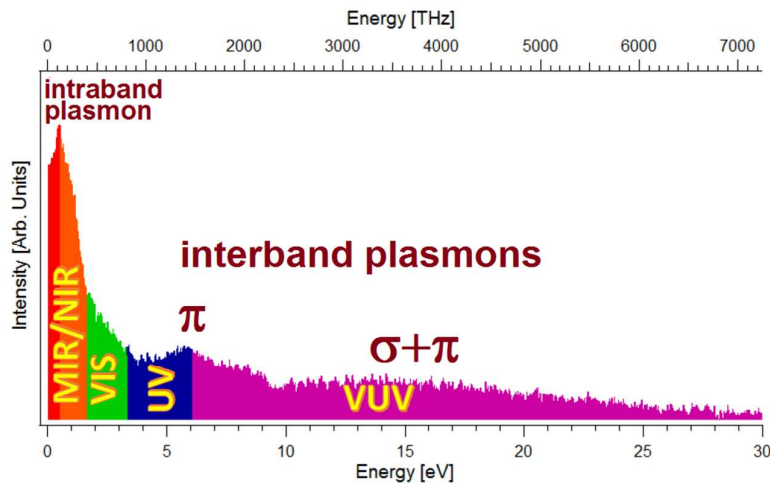
This is an *Accepted Manuscript*, which has been through the Royal Society of Chemistry peer review process and has been accepted for publication.

Accepted Manuscripts are published online shortly after acceptance, before technical editing, formatting and proof reading. Using this free service, authors can make their results available to the community, in citable form, before we publish the edited article. We will replace this *Accepted Manuscript* with the edited and formatted *Advance Article* as soon as it is available.

You can find more information about *Accepted Manuscripts* in the [Information for Authors](#).

Please note that technical editing may introduce minor changes to the text and/or graphics, which may alter content. The journal's standard [Terms & Conditions](#) and the [Ethical guidelines](#) still apply. In no event shall the Royal Society of Chemistry be held responsible for any errors or omissions in this *Accepted Manuscript* or any consequences arising from the use of any information it contains.

TABLE OF CONTENT



Plasmonic excitations of graphene (intraband and interband plasmons) and, moreover, composites modes formed by plasmons with other quasi-particles are reviewed

Plasmon modes in graphene: status and prospect

Antonio Politano^{1,} and Gennaro Chiarello^{1,2,*}*

1 Università degli Studi della Calabria, Dipartimento di Fisica, 87036 Rende (CS) Italy

2 Consorzio Nazionale Interuniversitario di Scienze Fisiche della Materia, via della Vasca Navale, 84, 00146 Roma, Italy

Abstract

Plasmons in graphene have unusual properties and offer promising prospect for plasmonic applications covering a wide frequency range, going from terahertz up to the visible.

Plasmon modes have been recently studied in both free-standing and supported graphene.

Here we review plasmons in graphene, with particular emphasis on plasmonic excitations in epitaxial graphene and on the influence of the underlying substrate on screening processes. Even if the theoretical comprehension of plasmons in supported graphene is still incomplete, several experimental results provide hints on the nature of plasmonic excitations in graphene on metals and semiconductors. Plasmon in graphene can be tuned by chemical doping and gating potentials. We show through selected examples that adsorbates may be used to tune the plasmon frequency, while the intercalation of chemical species allows to decouple the graphene sheet from the substrate, so as to recover the plasmon dispersion of pristine graphene. Finally, we will also report on intriguing effects due to many-body interaction, such as the excitations generated by electron-electron coupling (magnetoplasmons) and, moreover, the composite modes arising from the coupling of plasmons with phonons and with charge carriers.

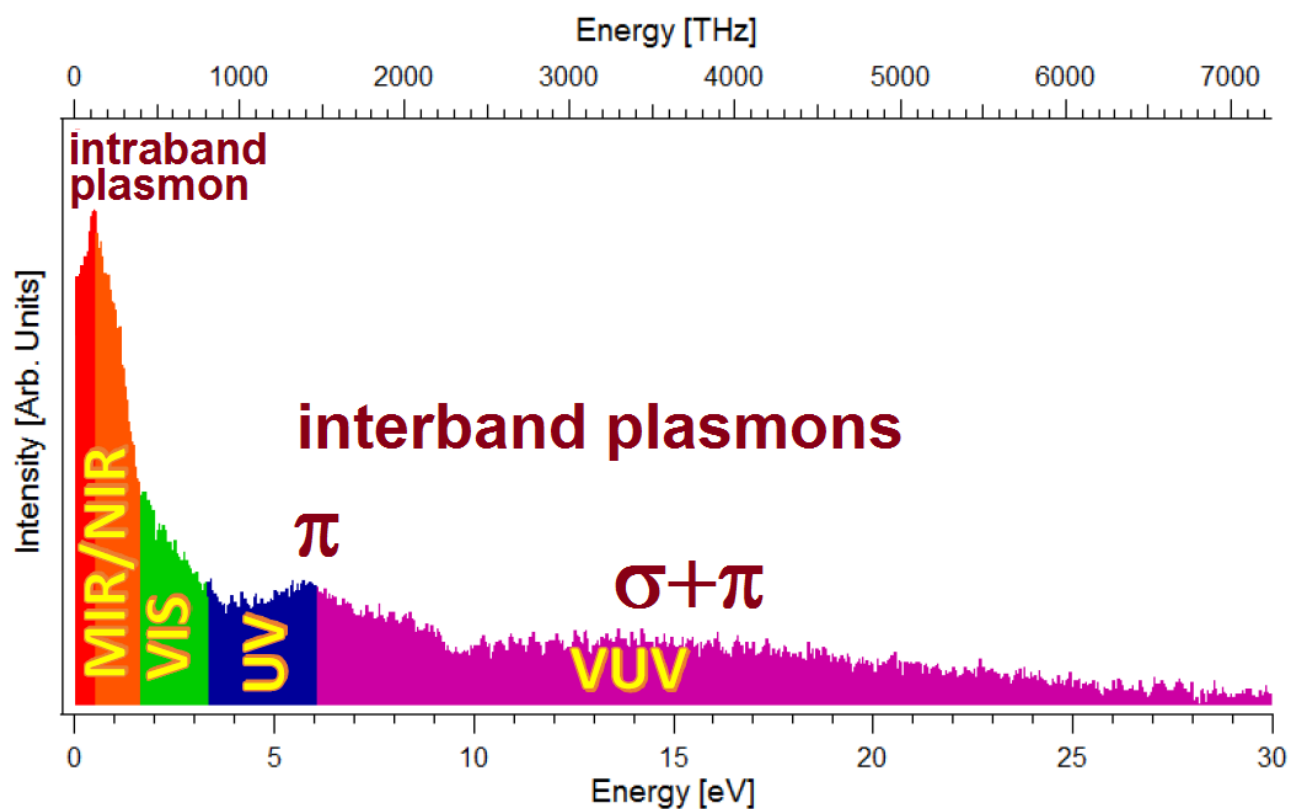
Keywords: plasmon, screening, epitaxial graphene, doped graphene, plasmonics, electron energy loss spectroscopy (EELS), plasmon-phonon coupling, plasmarons, magnetoplasmons

Address correspondence to:

antonio.politano@fis.unical.it (A. P.);

gennaro.chiarello@fis.unical.it (G. C.)

TABLE OF CONTENT



Plasmonic excitations of graphene (intraband and interband plasmons) and, moreover, composites modes formed by plasmons with other quasi-particles are reviewed

Introduction

Graphene is an innovative material, characterized by linearly dispersing π and π^* bands around the K point of the Brillouin zone, forming the so-called Dirac cone¹. Many of the peculiarities of massless Dirac fermions in graphene² are related to their collective excitations.

Plasmons are collective longitudinal excitations consisting in an oscillation of valence electrons³⁻⁵. Plasmons in graphene find important applications in optics⁶, microscopy⁷, nanolithography⁸, magneto-optic data storage⁹ and catalysis¹⁰. They are characterized by relatively long propagation distances¹¹, do not exhibit large Ohmic losses and can be confined to tighter regions¹². The linear dispersion of Dirac electrons enables ultrawideband tunability via electrostatic gating¹³.

Graphene is an ideal material for the emerging field of plasmonics¹⁴⁻²⁴. In fact, its versatility implies that graphene-based plasmonics may lead to the manufacture of innovative optical devices working in different frequency ranges—from terahertz to the visible—with extremely high speed, low driving voltage, low power consumption and compact sizes. As compared with silicon, graphene has higher thermal conductivity²⁵, high optical damage threshold²⁶ and important nonlinear optical properties²⁷ with subsequent higher potential for optoelectronic devices¹⁴. In particular, graphene plasmonics has important applications in light harvesting²⁸, optical biosensing²⁹, transformation optics³⁰, tunable metamaterials^{18, 23}, flexible waveguides³¹, and THz photodetectors³².

Recently, graphene has been combined with prefabricated plasmonic metamaterials³³ and plasmonic nanoarrays³⁴ to obtain tunable hybrid optical devices although the control of plasmon propagation at graphene/metal contacts is still unsatisfactory³⁵⁻³⁷.

Thus, understanding the behaviour of plasmon modes of graphene interfaced with substrates of different nature (oxides, semiconductors or metals) is mandatory for innovative applications. In particular, graphene-metal contacts³⁶⁻⁴⁵ are omnipresent and inevitable components of each graphene-based device and, thus, the investigation of the nature and dispersion of plasmon modes at graphene/metal interfaces is a key step toward engineering plasmonic applications of graphene. Recently, surface plasmon polaritons (SPPs) in graphene/metals have been used for engineering biosensors⁴⁶⁻⁴⁸. Moreover, interfacing graphene with a metal may also introduce novel properties in graphene, such as superconductivity (by proximity effects)⁴⁹⁻⁵¹ and magnetism⁵²⁻⁵⁵. Likewise, the formation of Schottky barriers at the interface of a zero-gap semiconductor (graphene) and conventional semiconductors⁵⁶⁻⁵⁸ may give rise to unusual physical phenomena and promising technological applications.

In this review, we will focus on the fundamental properties of plasmons in free-standing and epitaxial graphene. Moreover, we will review on the influence of adsorbates on graphene plasmons. We will also report on the coupling of plasmons with lattice vibrations (plasmon-phonon coupling) and with charge carriers (plasmareons).

Electron energy loss spectroscopy (EELS) is the main experimental technique for investigating collective electronic excitations (see Refs. ⁵⁹ and ⁶⁰ for a review on this technique).

In particular, while for photons only the long-wavelength region is accessible, EELS is able to scan an extended range in the reciprocal space (up to $0.4\text{-}0.5 \text{ \AA}^{-1}$)⁶⁰, so as to cover both the long- and the short-wavelength regions.

Plasmons in carbon-based materials

To put in evidence the peculiar properties of graphene plasmons, it is useful to briefly remind the properties of plasmons in carbon-based systems.

Plasmons in graphite originate from the collective excitations of the π valence electrons (π plasmon at 7–12 eV) and of all valence electrons (more intense and broader $\sigma+\pi$ plasmon at 28–33 eV).

For momentum transfers parallel to the graphite's surface, only interband transitions between states with same parity ($\pi \rightarrow \pi^*$ and $\sigma \rightarrow \sigma^*$) are allowed^{61, 62} (Figure 1). The π plasmon is originated by the $\pi \rightarrow \pi^*$ transition, which exhibits its maximum joint density of states (JDOS) near the M point of the Brillouin zone.

The same excitations are observed in nano-sized carbon materials, including fullerenes^{63, 64} and carbon nanotubes⁶⁵⁻⁶⁸.

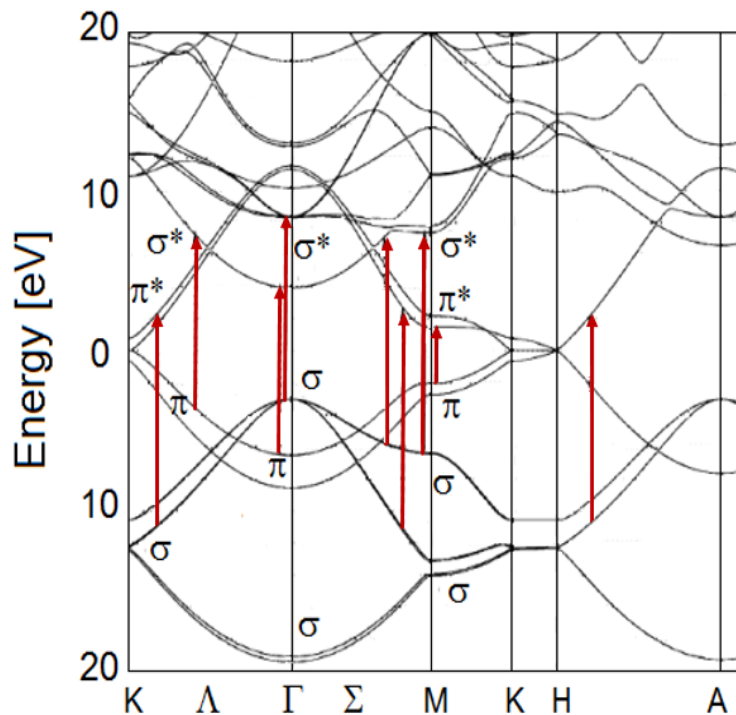


Figure 1. Kohn-Sham band structure of graphite along high-symmetry directions in the Brillouin zone.

Arrows indicate interband transitions. Adapted from Ref. ⁶⁹.

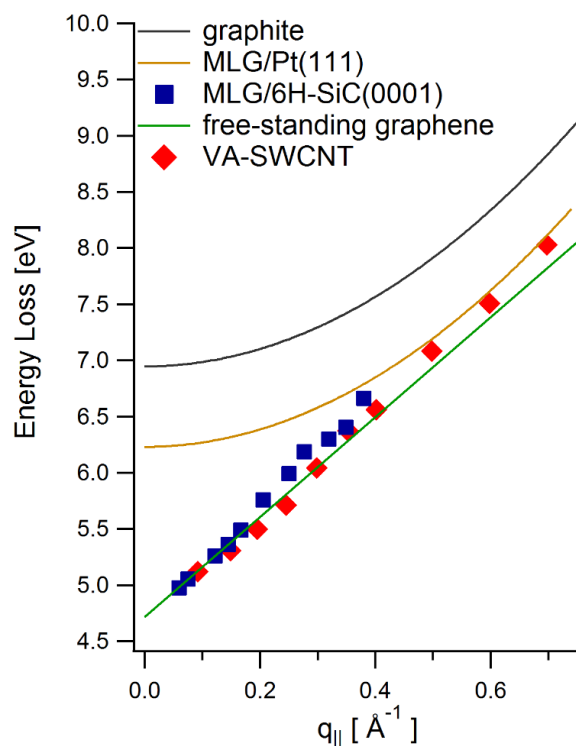


Figure 2. Dispersion of the π plasmon in graphite (gray line, data from Ref. ⁷⁰), VA-SWCNT (red diamonds, data from Ref. ⁷⁰), MLG/Pt(111) (orange line, data from Ref. ⁷¹), MLG/6H-SiC(0001) (blue squares, data taken from Ref. ⁷²) and free-standing graphene (green line, data from Ref. ⁷³).

The energy of the interband plasmon of π electrons in the long-wavelength limit ($q_{||} \approx 0$) is reported in Table I for various carbon-based systems, together with the full-width at half maximum (FWHM) of the plasmon peak. The energy of the π plasmon ranges between 4.7

eV (free-standing graphene)⁷⁰ and 6.5-7.0 eV (graphite)⁷⁴. Intermediate values have been recorded for vertically-aligned (VA) single-walled carbon nanotubes (SWCNT)⁷⁰ and monolayer graphene (MLG) on 6H-SiC(0001)⁷² (about 5 eV) and magnetically aligned bundles of SWCNT⁷⁵ (about 6 eV).

Table I. Energy and line-width of the π plasmon in the long wavelength limit (small momenta) for different systems

	$E_{\text{loss}} (q_{\parallel}=0)$ in eV	FHWM ($q_{\parallel}=0$) in eV
free-standing graphene (calculations ^{70,76} and experiments ⁶¹)	4.7 ⁶¹ ~ 6 ⁷⁶	0.45
MLG/6H-SiC(0001) ⁷²	4.9	0.95
VA-SWCNT ⁷⁰	5.1	1.00
Bilayer graphene on SiC(0001) ⁷²	5.3	1.10
Magnetically-aligned bundled SWCNT ⁷⁵	6.0	1.25
MLG/Pt(111) ⁷¹	6.2	1.40
3-4 layers graphene on SiC(0001) ⁷²	6.3	1.70
Graphite ^{74,77-79}	6.5 ^{74,77} ~ 7 ^{78,79}	2.90
MLG/Ni(111) ^{80,81}	6.7 ⁸¹ 7.5 ⁸⁰	~ 3

The broad $\sigma+\pi$ plasmon has an energy of 14.6 eV in monolayer graphene⁷². Both π and $\sigma+\pi$ plasmons exhibit a blue-shift by increasing the number of graphene sheets, as demonstrated for both free-standing membranes and for epitaxial graphene (Figure 3).

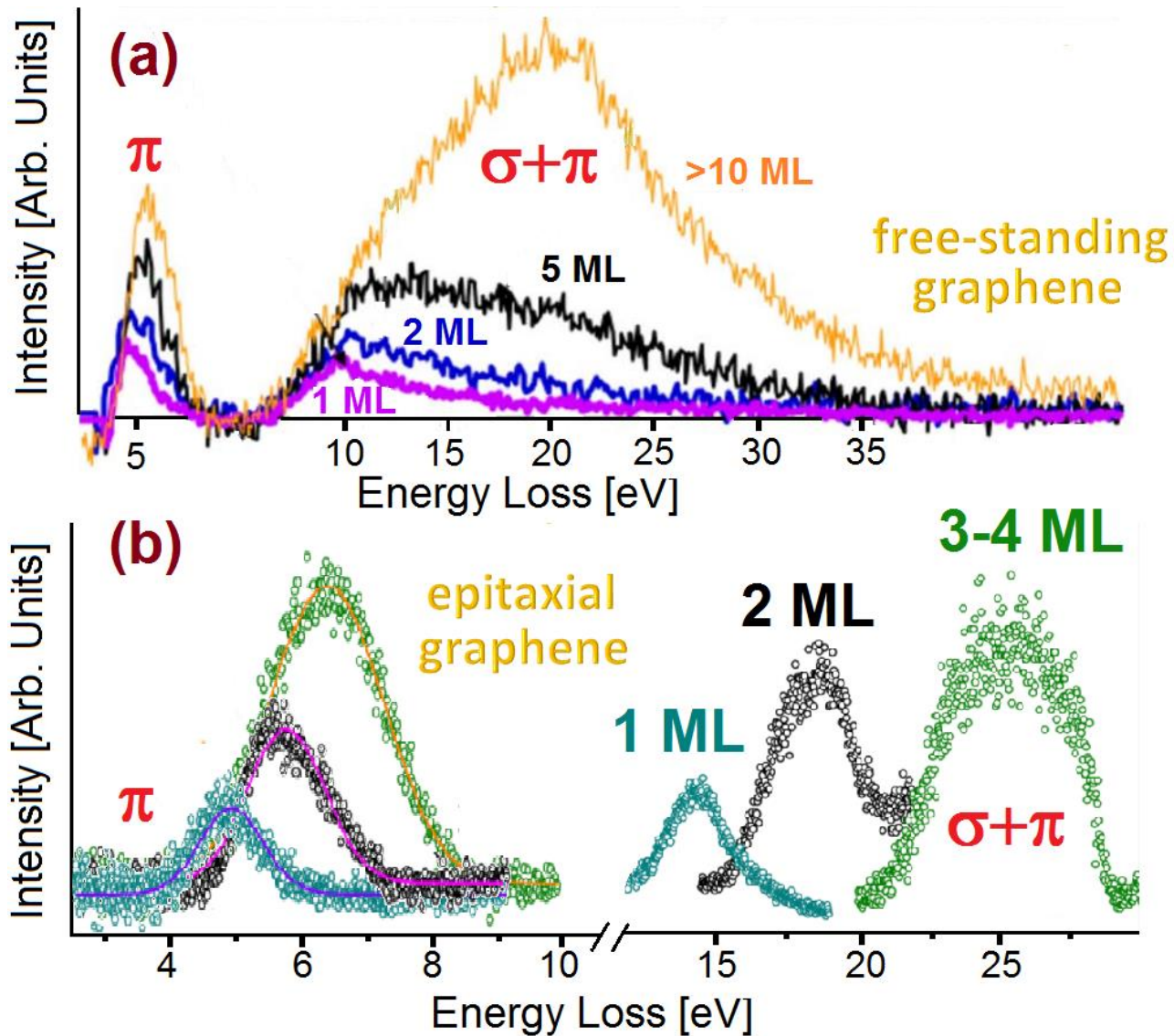


Figure 3. EELS spectra showing the dependence of π and $\sigma+\pi$ plasmons on the number of graphene layers for (a) a free-standing graphene membranes (adapted from Ref. ⁶¹); (b) graphene layers epitaxially grown on silicon carbide (adapted from Ref. ⁷²)

The red-shift of the energy of the π plasmon (at small momenta) when going from bulk graphite to quasi-two-dimensional graphene is caused by a decrease of the screening and of the interlayer coupling. This also influences the dispersion relation of the plasmon frequency. Linear dispersion of the π plasmon is found in VA-SWCNT⁷⁰, free-standing graphene^{70, 73} and MLG on 6H-SiC(0001)⁷² (Figure 2). The linear dispersion of the interband π plasmon in graphene and SWCNT is theoretically reproduced by inserting local field effects (LFE) in the electronic response⁷⁰.

On the other hand, quadratic dispersion of the π plasmon has been recorded in bulk graphite⁷⁴ and few-layer graphene on 6H-SiC(0001)⁷² with the same quadratic coefficient of the dispersion relation. For the latter system, it is evident that the realistic band structure of the system^{82, 83} changes the dispersion of the π plasmon from linear to quadratic as a function of the number of graphene layers.

In graphene/metal interfaces, the dispersion relation of the π plasmon is quadratic already for the MLG, as a consequence of the screening of the collective mode by the metal substrate. The screening in MLG on metal substrates is clearly more effective with respect to the case of graphene layers grown on the semiconductor silicon carbide substrate. This should explain the quadratic dispersion recorded in MLG/Ni(111) (Ref. ⁸¹) and MLG/Pt(111) (Ref. ⁷¹), in spite of the very different band structure of such two graphene/metal interfaces^{84, 85}. We also remind that the plasmon dispersion in the long-wavelength limit is predicted to be quadratic with respect to momentum for the interacting electron gas⁸⁶.

For the case of MLG/Ni(111), Cupolillo et al.⁸⁷ have suggested that the π plasmon is originated from transitions between interface states around K resulting from the graphene/Ni hybridization. Although the interface states responsible of such excitation are the consequence of a strong interaction with the substrate, the charge density associated to these states exhibits strictly 2D collective properties.

Intraband plasmon in doped graphene

Many theoretical studies address the collective electronic excitations in doped free-standing graphene⁸⁸⁻⁹⁰. In doped graphene, the dominant collective mode is the intraband or 2D plasmon. This mode has a crucial importance since the low energy of the intraband plasmon allows it to participate in many dynamical processes involving electrons and phonons⁹¹. The presence of the 2D plasmon is the main difference between collective excitations in pristine and doped graphene^{92, 93}. In doped graphene, the π^* band is partially filled and, thus, intraband transitions, not allowed in undoped graphene, are possible. The 2D plasmon can propagate undamped in the region delimited by the upper edge of the $\pi^* \rightarrow \pi^*$ intraband electron-hole continuum with the lower edge of the $\pi \rightarrow \pi^*$ electron-hole continuum. The two curves join for (k_F, E_F) where k_F is the Fermi wave-vector (see Figure 5). When the dispersion curve of the 2D plasmon enters in the $\pi \rightarrow \pi^*$ electron-hole continuum, it decays in single-particle excitations for the occurrence of Landau damping^{3, 94, 95}.

In the long wavelength limit ($q \rightarrow 0$) the 2D plasmon has the square-root-like dispersion of the two-dimensional electron gas (2DEG)⁹⁶⁻⁹⁹. However, at higher momenta the dispersion deviates from that of 2DEG, as a consequence of the onset of interband transitions along the Dirac cone. Such behavior can be reproduced by random-phase approximation (RPA) by including the effect of nonlocal field as a second-order correction:

$$\omega_{2D} = \left[\frac{4\pi n e^2}{m^*(1 + \epsilon_s)} |q| + \frac{3}{4} v_F^2 q^2 + \dots \right]^{1/2}$$

where n , m^* , and ϵ_s are the areal electron density, the effective mass and the static dielectric constant of the medium, respectively.

Graphene may be also intrinsically doped. As an example, graphene on SiC is naturally n -doped due to charge transfer from the substrate¹⁰⁰ while graphene/Pt(111) is p -doped⁸⁴. RPA has been used to reproduce the experimental dispersion of intraband plasmon of monolayer graphene on SiC. However, RPA can not accurately describe the plasmon dispersion (Figure 4) because of assumption of infinite relaxation time of electrons and the effect of many-body interactions¹⁰¹.

Detailed *ab initio* calculations by Despoja et al.⁹³ have indicated also an anisotropy of the 2D plasmon. In particular, in the Γ - M direction the dispersion curve follows the upper intraband edge, while in the Γ - K direction it is shifted toward higher energies (Figure 5).

This is a consequence of the anisotropy of π and π^* bands around the K point¹⁰²⁻¹⁰⁶.

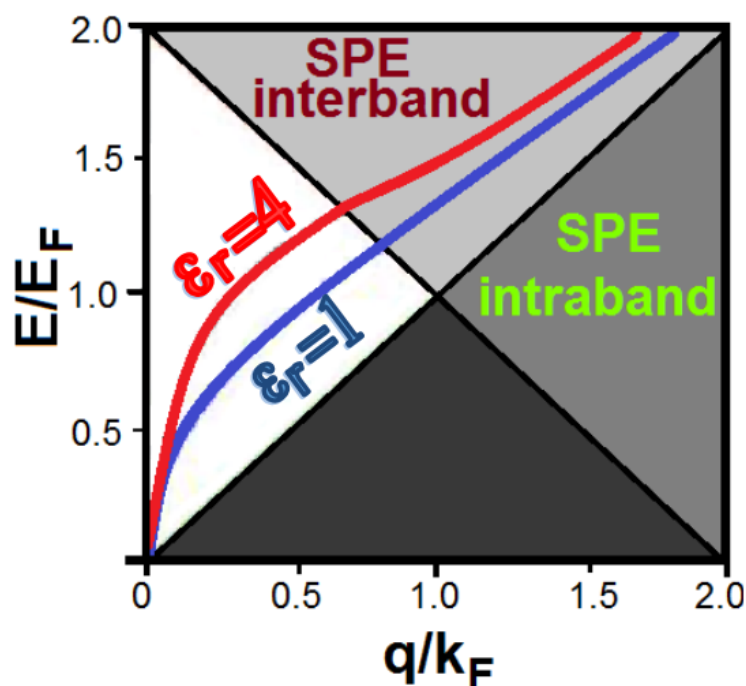


Figure 4. Dispersion relation of the 2D plasmon, as obtained by RPA calculations for (blue line) $\epsilon_r=1$ and (red line) $\epsilon_r=4$ where ϵ_r is the relative dielectric constant of the substrate underneath the graphene sheet. The dark grey (lower) and light gray (upper) shaded areas represent the continuum of intraband and interband excitations, respectively.

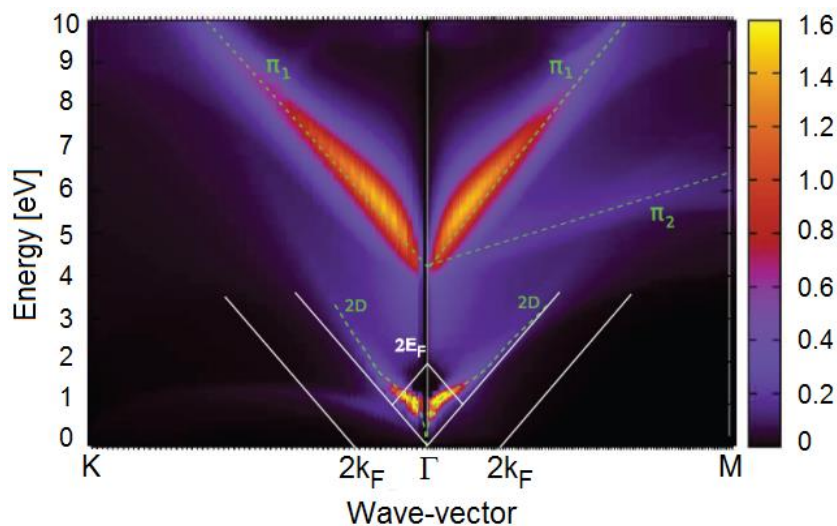


Figure 5. Intensities of electronic excitations in doped graphene ($E_F = 1$ eV). Adapted from Ref. ⁹³.

While a square-root-like dispersion of the intraband plasmon has been reported for free-standing graphene and graphene/SiC, experiments carried for monolayer graphene grown on metals measured a linearly dispersing intraband plasmon. In particular, measurements for graphene on Pt(111)¹⁰⁷⁻¹⁰⁹ and on Ir(111)¹¹⁰ have found a nearly identical dispersion relation (Figure 6).

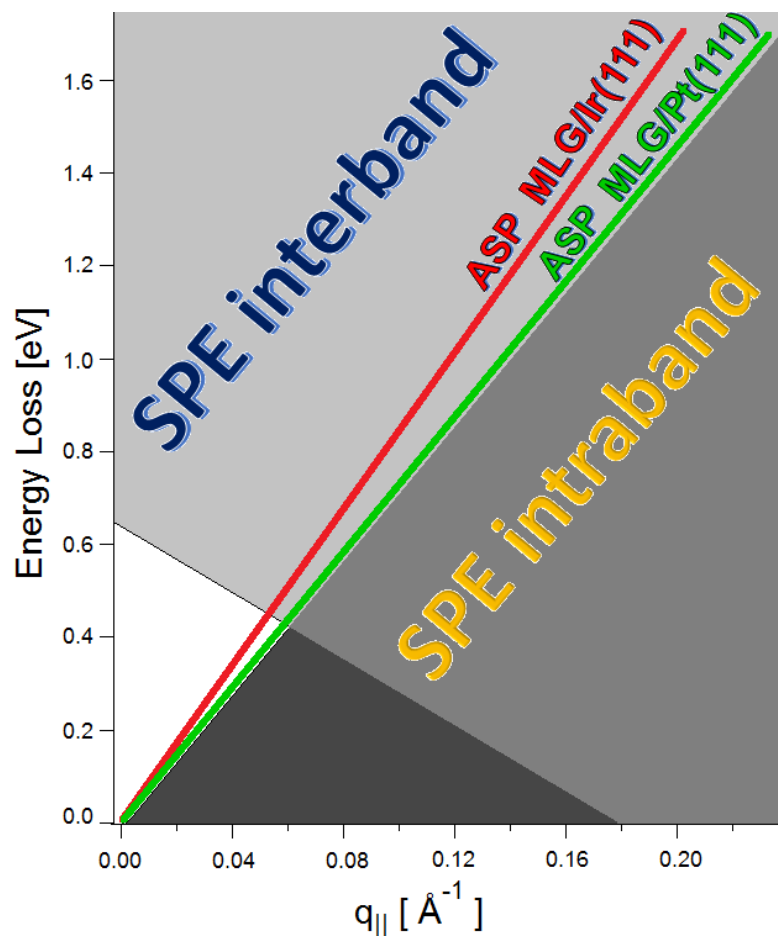


Figure 6. Dispersion relation of the ASP in MLG/Pt(111) (data taken from Ref. ¹⁰⁸) and MLG/Ir(111) (data taken from Ref. ¹¹⁰).

The linear dispersion of 2D plasmon in graphene/metal interfaces is a consequence of the coexistence of the metal electron gas with the π -charge density of graphene in the same spatial region. It resembles the acoustic surface plasmon (ASP) in metal surfaces with a partially occupied surface state band within a wide bulk energy gap^{111, 112}. The non-local character of the dielectric function¹¹³ and of the screening processes in graphene¹¹⁴ prevents the sheet plasmon from being screened out by the 3D bulk states of the metal substrate.

The group velocity of intraband plasmon in MLG/metals ($\approx 10^6$ m/s), extracted from the slope of the dispersion relation, is similar to those ones calculated for ASP, thus indicating a similar nature of the two collective excitations.

The group velocity of the sheet plasmon in MLG/metals is about two orders of magnitude lower than the speed of light, and thus its direct excitation by light is not possible. However, nanometer-size objects at surfaces, such as atomic steps or molecular structures, can allow coupling between sheet plasmon and light. The linear behavior of its dispersion implies that both phase and group velocities of the collective excitation are the same, so signals can be transmitted undistorted along the surface with potential applications in graphene-based nano-optical devices.

By contrast, in MLG/Ni(111) localized interface states support an ordinary 2D plasmon with square-root-like dispersion¹¹⁵.

In addition to the ordinary intraband plasmon, a few recent theoretical works show the existence of a nonlinear plasmon in free-standing doped graphene^{116, 117}. Although a similar excitation has been observed also experimentally^{109, 118} (see the nonlinear mode in Figure 13), its origin is still unclear and currently under investigation. In particular, the intensity of this mode increases with applied strain¹¹⁷, in contrast with the behavior of the intraband plasmon, which is not influenced by uniaxial strain¹¹⁷.

To put in evidence the effects of interlayer interactions, interband plasmons have been studied also in bilayer graphene by theoreticians. Two plasmon modes are predicted in the long-wavelength limit (Figure 7): the first one is characterized by a square-root-like dispersion (ω_+) while the other is an acoustic plasmon (ω_-)¹¹⁹⁻¹²². The dispersion relation of these modes depend on the interlayer distance (d) and on the electron concentrations of the two layers (n_1 and n_2). For the sake of truth, theoretical models reporting a single low-energy plasmon mode in bilayer graphene are also present¹²³.

The co-existence of 2D plasmons (\sqrt{q} dispersion) with ASP (linear dispersion) in bilayer graphene resembles the case of inversion layers on semiconductor surfaces (see, e.g., the work on InAs(110) by H. Yu et al¹²⁴). In this system the ASP dispersion originates as well from the interplay of two quantum well minibands.

Unfortunately, experimental investigations on low-energy plasmons in bilayer graphene are still lacking.

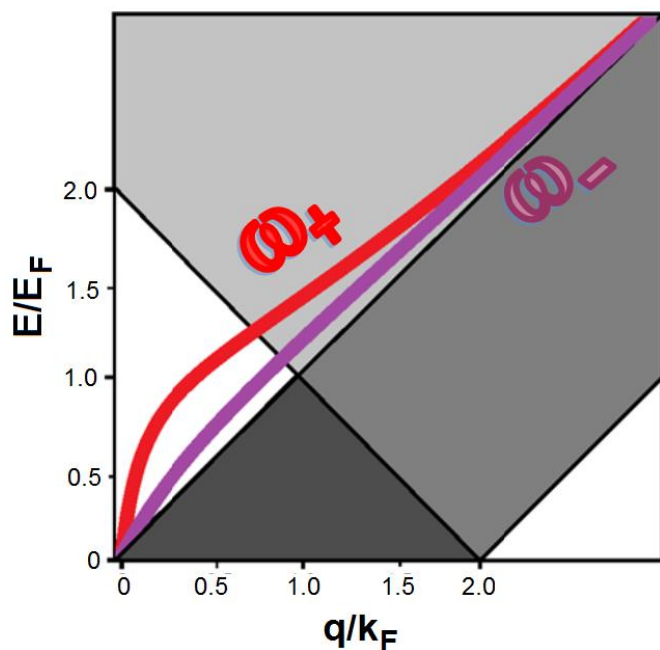


Figure 7. Dispersion relation of plasmon modes in bilayer graphene (shown for the case of an *AA*-stacking, adapted from Ref. ¹²¹). In the long wavelength limit, the ω_+ mode has a square-root-like dispersion while an acoustic dispersion is found for the ω_- mode (see Ref. ¹²⁵ for more details).

Influence of adsorbed and intercalated atoms

The tunability of graphene plasmons is a promising opportunity for the emerging field of graphene-based plasmonics. Both the conductivity of graphene and the dispersion of plasmons in graphene are related to Fermi energy (or chemical potential at room temperature). The Fermi energy

$$E_F \approx \mu \approx \sqrt{\pi \hbar^2 v_F^2 n}$$

can be easily controlled (with a subsequent tuning of plasmon modes) by changing the charge concentration, which, in turn, can be realized by gating potentials or chemical doping¹²⁶.

In view of possible applications, it should be mentioned that distributing carriers into multiple graphene/insulator stacks efficiently enhances the plasmonic resonance frequency and its magnitude¹²⁷.

High electropositive or electronegative chemical species can easily dope graphene due to charge transfer. In Figure 8, results for K-doped graphene/SiC¹²⁸ are reported. With the addition of more electrons in the π^* band, the Fermi level shifts upward away from the Dirac point E_D and this causes a continuous blue-shift of the plasmon energy with increasing potassium coverage.

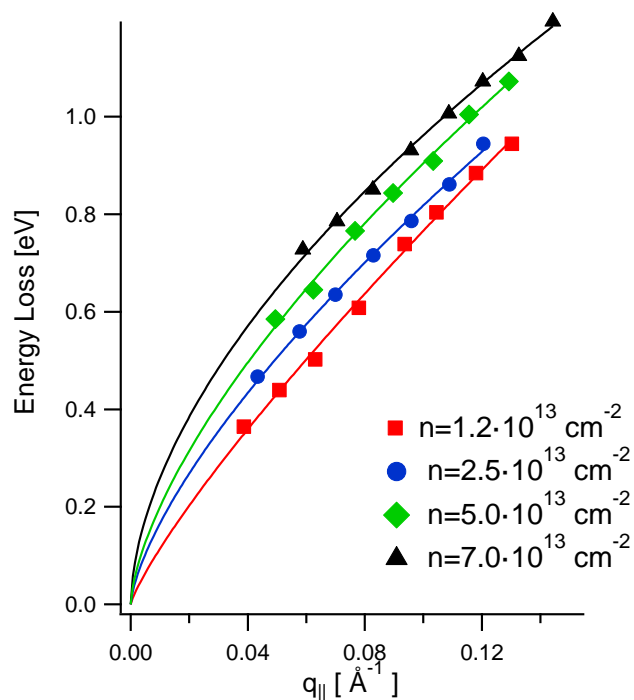


Figure 8. Dispersion relation of the intraband plasmon for different amounts of the electron density n . The intraband plasmon excitation arising from intrinsic electron density $n = 1.2 \cdot 10^{13} \text{ cm}^{-2}$ changes when more electrons are added by K doping. Adapted from Ref. ¹²⁸.

Likewise, a red-shift has been reported in water-exposed MLG/Pt(111)¹⁰⁷. However, in the latter study, charge doping affects the frequency of the plasmon modes but not the acoustic behaviour of the dispersion relation. Nevertheless, a reduction of the group velocity by about 11% has been observed¹⁰⁷.

By contrast, experiments performed for Na-doped MLG/Ir(111)¹¹⁰ and F4-TCNQ/MLG/SiC¹²⁹ by Pfnür's group show negligible influence of doping on the dispersion curve while noticeable changes in the damping mechanisms of the plasmon modes are reported.

Interesting results have been reported for plasmon dispersion in Cs-intercalated graphene/Ni(111)¹³⁰. Graphene on Ni(111) exhibits a strong hybridization between Ni d bands and π states of graphene^{131, 132}. Intercalated chemical species may decouple the graphene sheet from the substrate¹³³⁻¹³⁵. The influence of intercalated atoms on the electronic structure of the MLG/Ni(111) would reflect itself in the collective electronic properties of the intercalated system. The dispersion curve of π plasmon, in comparison with the analogous dispersion curve obtained in the absence of intercalated Cs, shows that alkali metal atoms make graphene to be quasi-freestanding, with a much lowered charge transfer, and with the recovery of the linear dispersion typical of free-standing graphene (Figure 9).

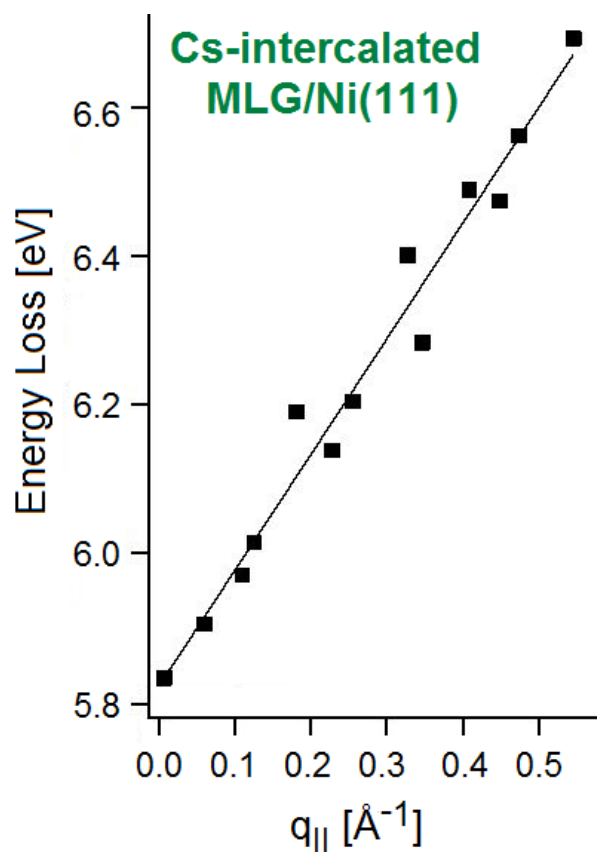


Figure 9. Plasmon dispersion for Cs-intercalated graphene/Ni(111). The linear dispersion of the π plasmon in pristine, free-standing graphene is recovered (see Figure 2 for comparison). Adapted from Ref. ¹³⁰.

Plasmon modes may be influenced also by the p -type doping arising from the interaction of the graphene/metal interface with atmosphere¹³⁶. Thus, the atmospheric doping should be taken into account when engineering of graphene-based devices which should work under realistic conditions, i.e. in air. To investigate the stability in ambient air humidity of the contacts between metallic electrodes and graphene, Politano and Chiarello have probed plasmon modes in air-exposed graphene/metal contacts^{36, 37}. For the case of MLG/Ru(0001), both the intraband and the interband π plasmons are quenched once that the sample was exposed to atmosphere (Figure 10). This finding indicates that in graphene/Ru(0001) π bands are disrupted upon interaction with ambient air humidity with the appearance of a band gap. Scanning tunneling microscopy (STM) results in Ref. ¹³⁷ support this picture.

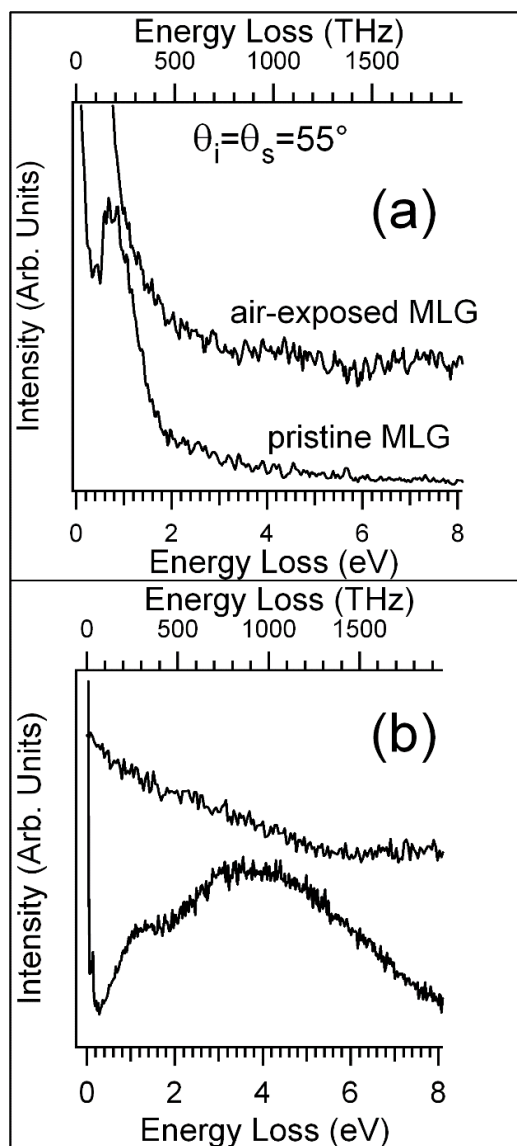


Figure 10. (a) EELS spectra, recorded in specular geometry (incidence angle of 55° with respect to the sample normal) and at room temperature for pristine MLG/Ru(0001) (bottom spectrum) and the air-exposed sample (top spectrum); (b) EELS spectra, acquired in off-specular geometry and at room temperature for pristine MLG (bottom spectrum) and the air-exposed sample (top spectrum). The primary electron beam energy is 20 eV. Two energy scales are reported in eV (bottom axis) and THz (top axis).

By contrast, plasmons in graphene-Pt contacts exposed to air behave differently with respect to graphene-Ru contacts. In details, the intraband plasmon in graphene/Pt(111) (Figure 11) undergoes a red-shift from 2.5 to 1.6 eV upon air exposure due to *p*-type atmospheric doping^{138, 139}, estimated to be $\sim 3 \cdot 10^{12} \text{ cm}^{-2}$ in this case.

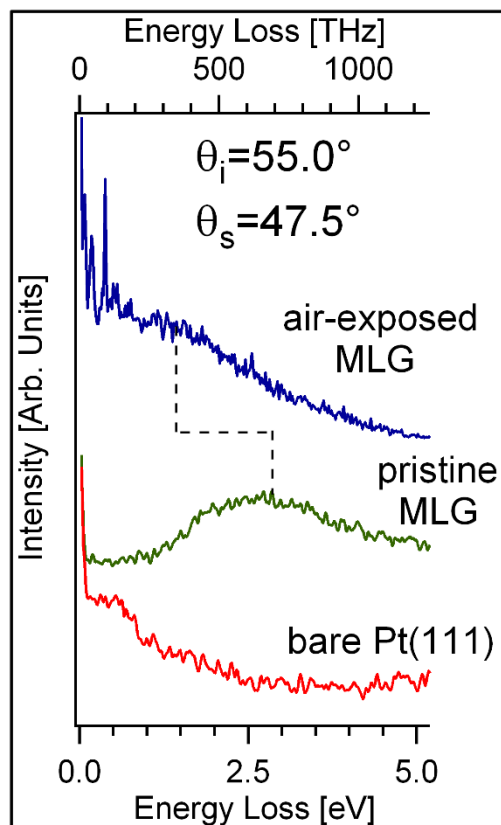


Figure 11. EELS spectra recorded for bare Pt(111), pristine MLG/Pt(111), and the air-exposed MLG/Pt(111) sample. The incidence angle is 55.0° while the scattering angle is 47.5° . EELS measurements and air exposure have been performed at room temperature. The primary electron beam energy is 20 eV.

In both graphene/metal contacts, vibrational spectra of air-exposed samples show the presence of C-H groups^{36, 37, 140-142}, likely arising from the dissociation of water molecules on the underlying metal catalyst with the subsequent H spillover^{141, 142}.

Therefore, plasmonic devices can be strongly affected by ambient humidity, in contrast with too optimistic predictions¹⁴³ based on the assumption that graphene is chemically inert. However, the chemical inertness of graphene may be realistic when considering free-standing, undefected graphene membranes but the scenario may be completely different for epitaxial graphene, where the underlying substrate acts as a catalyst toward water^{36, 37, 140-142} in ambient air humidity.

While H-induced band opening was reported on MLG grown on Ir(111)¹⁴⁴ and Au-intercalated Ni(111)¹⁴⁵, no bandgap exists in hydrogenated graphene on Pt(111)¹⁴⁶. Hence, hydrogenation of graphene on metals may induce the opening of a band gap (Ru, Ir, Ni substrates) or it may result in an increased metallic character through hybridization with the underlying substrate as on Pt(111)¹⁴⁶. This would explain the survival of plasmon modes in air-exposed graphene-Pt contact (Figure 11).

Confinement of π plasmon

Plasmon confinement has been found to occur in graphene/Ru(0001)¹⁴⁷. In this system, the graphene sheet is not perfectly flat but it exhibits ripples in which electronic properties are periodically inhomogeneous^{148, 149}. Ripples are separated by each other by about 3 nm^{148, 150, 151}. Height and width of these ripples are consistent with models which allow the carbon atoms to form different types of bonds with the underlying substrate. In particular, carbon atoms located at the higher areas of the superstructure are adsorbed on three-fold sites (fcc, hcp) and they scarcely interact with the substrate. Instead, carbon atoms closer to the Ru substrate occupy hcp and on-top positions and form a strong chemical bond with Ru. In the latter case, a strong hybridization between $2p_z$ states of carbon atoms and the $4d_z^2$ orbitals of Ru¹⁵² occurs.

The π -plasmon frequency of MLG/Ru(0001) remains nearly constant up to a critical wavevector q_c ($\approx 0.30 \text{ \AA}^{-1}$, Figure 12). This finding contrasts with previous experimental results attained for graphene grown on Pt(111)⁷¹ and SiC(0001)⁷² and for bulk graphite⁷⁴ (see Figure 2). The dispersionless behaviour of the frequency found in MLG/Ru(0001) for $q_{||} < q_c$ ($q_c \approx 0.30 \text{ \AA}^{-1}$) is a fingerprint of the occurrence of plasmon confinement¹⁵³⁻¹⁵⁵, i.e. valence electrons oscillate independently in the single graphene quantum dot of diameter $d = 2\pi/q_c$. In the present case, d results to be $21 \pm 3 \text{ \AA}$, in excellent agreement with STM experiments^{148, 151, 156}.

Thus, the existence of ripples has strong and evident effect on the localization and dispersion of the π plasmon. Propagation of the plasmon mode occurs only for wavelengths smaller than the average size of the ripples. For $q_{||} > 0.30 \text{ \AA}^{-1}$ (shorter wavelength) the frequency of the π plasmon rapidly increases.

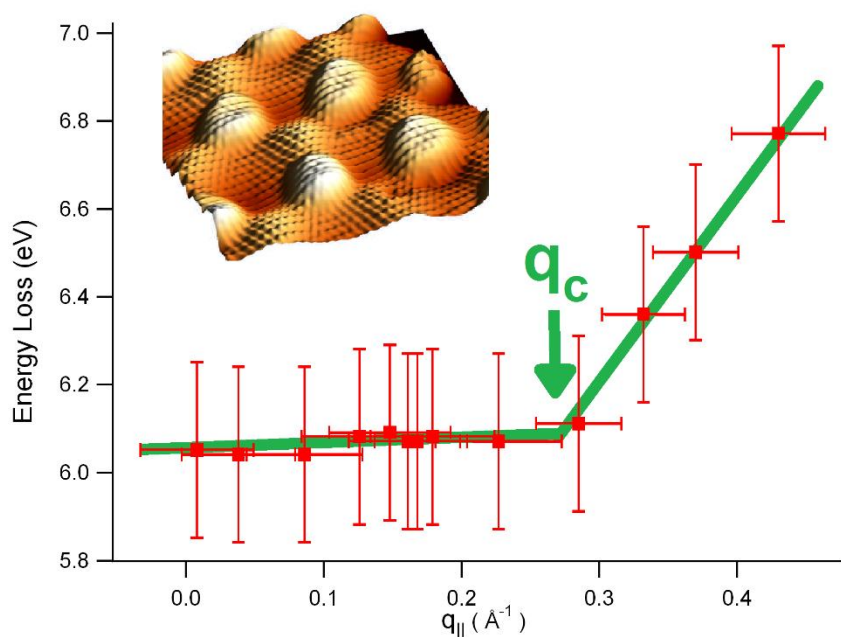


Figure 12. Dispersion relation of π plasmon in periodically rippled graphene/Ru(0001). The inset shows a 3D representation of STM image of nanodomains in MLG/Ru(0001), based on the STM study in Ref.¹⁴⁸.

Influence of roughness

Roughness has immediate influence on plasmon lifetime. At fixed plasmon wavelength, the lifetime is inversely proportional to the step concentration. Thus, steps induce strong damping of the plasmonic excitation. For a given roughness, the line-width of the plasmon peak increases for decreasing plasmon wavelength. Hence, the lifetime is proportional to the step density and plasmon wavelength ($\tau \approx \lambda_{pl} \cdot \Gamma$)¹⁵⁷.

Plasmon-phonon coupling

The coupling of phonons with plasmons has direct effect on plasmonics and on transport¹⁵⁸ properties.

Plasmon-phonon coupling is a striking manifestation of the breakdown of the Born-Oppenheimer approximation¹⁵⁹. The plasmon-phonon coupling phenomenon implies the hybridization of the plasmon modes of the 2DEG with the optical phonon modes of the lattice, giving rise to the coupled plasmon-phonon modes.

Plasmon-phonon coupling in graphene has been predicted by Jablan et al.¹⁵⁹ (by using the self-consistent linear response formalism) and experimentally observed for quasi-freestanding graphene on Pt(111)¹⁰⁹. The ASP couples with the out-of-plane (ZO) and the transverse (TO) optical phonons of the graphene. Such coupling can occur only in the long-wavelength limit ($q_{||} \sim 0$), for which the frequency of the sheet plasmon is in the same energy scale to those ones of the optical phonons.

These modes have mixed phonon and plasmon characteristics. Referring to Fig. 13, for high momenta the composite modes at 100 and 200 meV have the characteristics of phonon modes and converge to the frequency of the ZO and TO modes, respectively. In the long-wavelength limit, the energy of the composite mode goes to zero and thus behaves as a pristine 2D plasmon mode.

However, the intraband plasmon of graphene may also couple to surface optical phonons of a polar substrate, as observed for Fuchs-Kliwer phonons of SiC¹⁶⁰ and SiO₂¹⁶¹ (Figure 14).

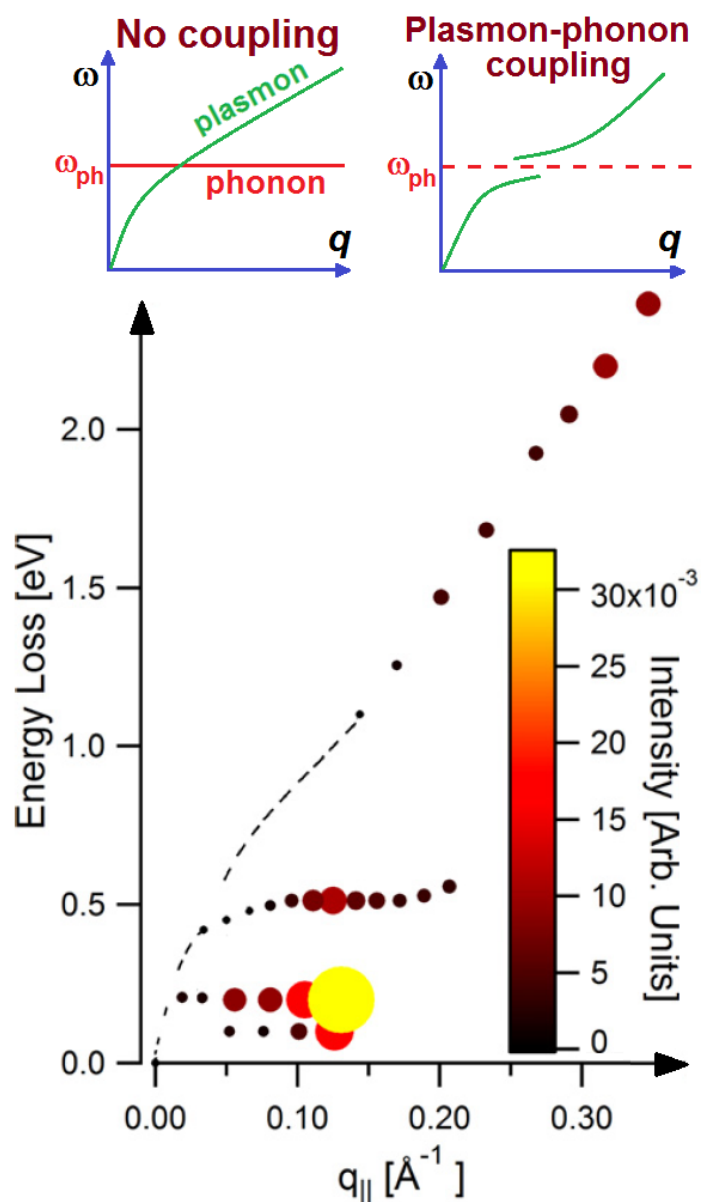


Figure 13. Dispersion relation of collective excitations in MLG/Pt(111). Note that the existence of composite modes has a striking dependence on kinematic conditions, which should be chosen carefully to put in evidence such effects. The influence of plasmon-phonon coupling on the dispersion relation of plasmon modes is sketched in the top part of the figure. The nonlinear mode dispersing from 0.4 to 0.6 eV has an unclear origin. It has been suggested that such mode can be originated by trigonal warping in the Dirac cone of graphene¹¹⁶.

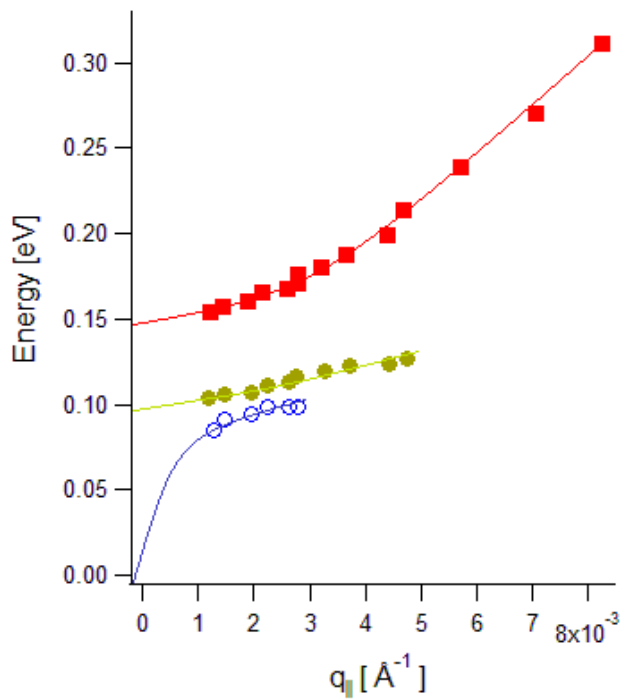


Figure 14. *Plasmon dispersion in graphene on SiO₂. Adapted from Ref. ¹⁶¹.*

Plasmarons

Originally, the concept of “plasmaron” has been introduced to indicate the plasmon-phonon hybrid state. More recently, it has been re-introduced with a slightly different, but likely more general meaning: not only a phonon dressed by plasmons, but also other plasmon-dressed elementary excitations are named plasmarons. Based on angle-resolved photoemission spectroscopy (ARPES) results for K-doped graphene on silicon carbide¹⁶², several researchers have claimed the occurrence of plasmarons in graphene¹⁶²⁻¹⁶⁸, defined as particles dressed by density oscillations of the electron gas. The Dirac crossing point is resolved into three crossings: the first between pure charge bands, the second between pure plasmaron bands, and the third a ring-shaped crossing between charge and plasmaron bands (Figure 15).

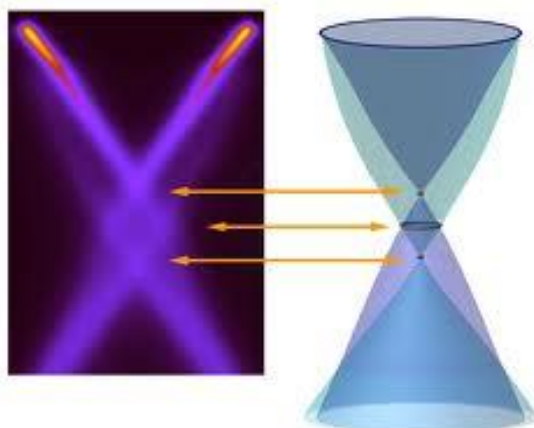


Figure 15. *ARPES results for K-doped graphene in Ref. ¹⁶² reveal that the energy bands of ordinary charge carriers (holes) meet at a single point, but conical bands of plasmarons meet at a second, lower Dirac crossing. Between these crossings lies a ring where the hole and plasmaron bands cross. The new band picture has been used to claim a strong coupling of plasmons with charge carriers in graphene¹⁶²⁻¹⁶⁸.*

However, this picture has been recently questioned by Lischner et al.¹⁶⁹. They demonstrate that an innovative treatment of electron correlations with an ab initio GW plus cumulant theory together with an careful description of the substrate screening well reproduce experimental results in Ref. ¹⁶².

No substrate induced band gap or a plasmaron solution can be found within this advanced theoretical approach. Thus, it is now definitively clarified that the lack of sufficient electron correlations at the GW level leads to an extra solution to Dyson's equation so as to overestimate the quasiparticle-satellite separation.

Magnetoplasmons

Recently, magnetoplasmonics is attracting huge interest for its potential applications in technology^{170, 171}. The 2D magnetoplasmons are collective excitations between Landau levels¹⁷² due to electron-electron interactions, which can be observed through infrared optical absorption and inelastic light scattering¹⁷³⁻¹⁷⁸. In layered and doped graphene structures, the instability and unusual dispersion of magnetoplasmon modes have been studied in recent years, within different approaches^{172, 179-195}. Magnetoplasmons have been observed in graphene epitaxially grown on SiC¹⁹⁶. The Drude absorption is transformed into a strong terahertz plasmonic peak due to nanoscale inhomogeneities, such as substrate terraces and wrinkles. Plasmonic excitations also modify the magneto-optical response and, in particular, the Faraday rotation¹⁹⁶. This makes graphene a unique playground for plasmon-controlled magneto-optical phenomena thanks to a cyclotron mass 2 orders of magnitude smaller than in conventional plasmonic materials, such as noble metals.

The field-induced splitting of the plasmon peak resembles strikingly the appearance of collective resonances observed previously in other systems¹⁹⁷⁻²⁰⁰. The upper and lower branches are attributed to the so-called bulk and edge magnetoplasmons, respectively, with the frequencies

$$\omega_{\pm} = \sqrt{\frac{\omega_c^2}{4} + \omega_0^2} \pm \frac{|\omega_c|}{2}$$

where ω_0 is the plasmon frequency at zero field, $\omega_c = \pm eB/mc$ is the cyclotron frequency, defined as positive for electrons and negative for holes, m is the cyclotron mass, and c the speed of light. At high fields ($|\omega_c| \gg \omega_0$), the upper branch becomes essentially the usual cyclotron resonance with a linear dependence on magnetic field, while the lower branch represents a collective mode confined to the edges²⁰¹ with the energy inversely proportional to the field (Figure 16).

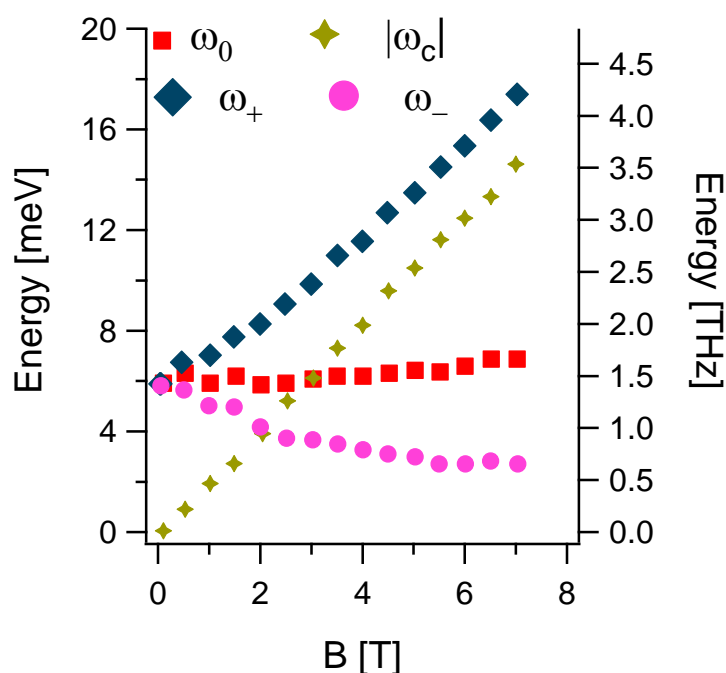


Figure 16. Dependence of the plasmon energy ω_0 , the cyclotron resonance energy ω_C and the magnetoplasmon energies ω_{\pm} on the magnetic field B . Adapted from Ref. ¹⁹⁶.

Coupling of plasmons with photons

The capability to handle optical fields and the energy flow of light is crucial in communication and information technologies. However, the electric control of light is not possible, since photons are chargeless. Plasmon polaritons, coupled excitations of photons and plasmons, in graphene offers an opportunity to achieve electric control of light.

Recently, graphene plasmons have been imaged by Fei *et al.*²⁰² and Chen *et al.*²⁰³. These authors used the tip of an atomic force microscopy (AFM) probe in a scattering-type scanning near-field optical microscopy (s-SNOM) setup to excite and image graphene plasmons in real space (Figure 17).

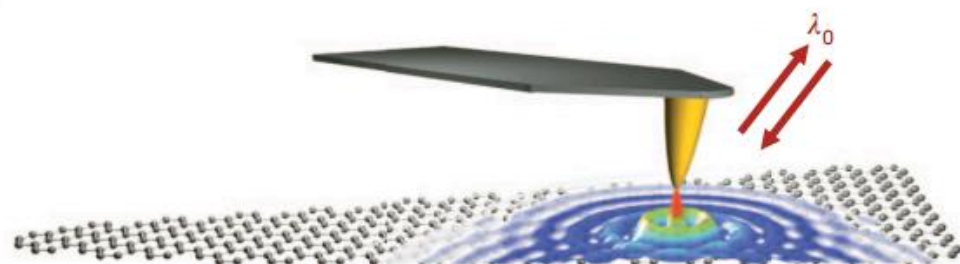


Figure 17. Sketch of the experimental setup used for launching and imaging graphene plasmons (represented as blue rings). The metallized AFM tip (shown in yellow) is illuminated by an infrared laser beam with wave-length λ_0 . Taken from Ref. ²⁰³

By reducing the degree of freedom, SPPs can propagate in wanted direction in ribbons, which act as waveguides¹¹.

Infrared light polarized perpendicular to the ribbon axis can excite SPPs in graphene¹⁸. Plasmon excitations in the graphene micro-ribbon array can be varied by electrical gating and the plasmon frequency scales as $W^{-1/2}$, where W is the width of the ribbon. The graphene plasmonic waveguides based on microribbons is able to transmit up to 2.5 Gbps optical signals³¹.

An additional handle to control plasmon excitations is provided by the dielectric environment and the relative arrangement of the interacting waveguides. Plasmon interaction and hybridization in pairs of neighboring aligned ribbons are strong enough to produce dramatic modifications in the plasmon field profiles¹¹.

Plasmon propagation in graphene-based circuits can be tailored by introducing nanoscale discontinuities, either by graphene patterning or by tailoring the substrate topography²⁰⁴. To reduce the dimensionality further, graphene plasmons have been studied also in nanodisks²⁰⁵ or nanorings²⁰⁶. Localized plasmon resonance in nanodisks becomes very strong and causes a strong enhanced electrical field. This allows to achieve a sufficiently strong coupling with an adjacent quantum emitter (quantum dot or a molecule) to give rise to *plasmon blockade*²⁰⁵ effect, characterized by nonlinear absorption cross section and modified statistics of the bosonic plasmon mode²⁰⁵.

Other promising prospect of applications arises from heterostructures. Using patterned graphene/insulator stacks¹²⁷, it is possible to realize tunable infrared plasmonic devices to be used as detectors or modulators.

Conclusions and outlook

Graphene plasmons show very promising properties which can be used for applications: reasonably large life-times, tunability of the plasmon frequency, electric controllability, plasmon confinement and strong coupling with phonons and light.

Graphene could represent an ideal playground for applications of two-dimensional electromagnetic waves²¹, so as to facilitate the design and miniaturization of nanophotonic devices¹¹.

Recently, plasmonics has having groundbreaking impact in photonics²⁰⁷. Plasmonics has opened the way for the realization of high-speed and transparent photosensitive systems, which could be further functionalized to enable chemical sensing¹³. The combination of graphene with conventional plasmonic elements will allow the realization of THz plasmonic lasers²⁰⁸⁻²¹⁰, plasmonic antennas²¹¹, plasmonic waveguides^{31, 212, 213}, Luneburg lenses³⁰, ultrasensitive biosensors^{29, 46, 48, 214, 215} and so on. The flexibility of graphene²¹⁶ may permit the realization of graphene-based flexible plasmonic devices²⁰. Moreover, the largely non-linear optical response of graphene²⁷ can allow innovative experiments and applications of graphene-based nonlinear plasmonics^{217, 218}.

However, there are still some limitations and open problems for graphene-based plasmonics, as for example the lack of reliable THz light sources.

This overall encouraging viewpoint for applications is also accompanied by the possibility to carry out many other fascinating fundamental studies. As an example, accurate experimental studies on plasmons in bilayer graphene on metals would be essential to verify and improve current theoretical models for both plasmon dispersion¹¹⁹⁻¹²² and plasmaron formation^{163, 166}. Screened electron-electron interactions in a graphene sheet supported by a metal substrate are responsible for intriguing many-body effects. Despite the strong screening exerted by the metal, the 2DEG in graphene/metals contacts shows self-sustaining, long-living oscillations whose phase velocity coincides with the group velocity (ASP). Concerning high-energy plasmons (e.g., the π plasmons at 5-7 eV), they are suitable candidate for potential applications in UV regions in composite structures with materials able to emit or absorb UV light. However, accurate theoretical models for plasmons graphene/metal interfaces are still missing due to the difficulty in the theoretical description of the screening by the underlying metal substrate. The out-of-plane charge transfer between graphene and the metal is determined by the difference between the work function of graphene and the metal surface and, in addition, by the metal-graphene chemical interaction that creates an interface dipole which lowers the metal work function. The induced electrostatic potential decays weakly with the distance from the metal contact as $V(x) \approx x^{-1/2}$ and $\approx x^{-1}$ for undoped and doped graphene, respectively²¹⁹. Instead, current models overestimate the screening by the metal substrate. Likely, the experimental study of plasmons in graphene supported by jellium surfaces could help theoreticians to improve our understanding of screening processes at graphene/metals. Unfortunately, such experimental study is complicated by the difficult preparation of graphene on aluminum.

References

1. A. H. Castro Neto, F. Guinea, N. M. R. Peres, K. S. Novoselov and A. K. Geim, *Rev. Mod. Phys.*, 2009, **81**, 109-162.
2. K. S. Novoselov, A. K. Geim, S. V. Morozov, D. Jiang, M. I. Katsnelson, I. V. Grigorieva, S. V. Dubonos and A. A. Firsov, *Nature*, 2005, **438**, 197-200.
3. J. M. Pitarke, V. M. Silkin, E. V. Chulkov and P. M. Echenique, *Rep. Prog. Phys.*, 2007, **70**, 1-87.
4. J. Yan, Z. Yuan and S. Gao, *Phys. Rev. Lett.*, 2007, **98**, 216602.
5. H. Qin, Y. Gao, J. Teng, H. Xu, K. H. Wu and S. Gao, *Nano Lett.*, 2010, **10**, 2961-2964.
6. A. V. Zayats, I. I. Smolyaninov and A. A. Maradudin, *Phys. Rep.*, 2005, **408**, 131-314.
7. A. R. Halpern, J. B. Wood, Y. Wang and R. M. Corn, *ACS Nano*, 2014, **8**, 1022-1030.
8. W. Srituravanich, N. Fang, C. Sun, Q. Luo and X. Zhang, *Nano Lett.*, 2004, **4**, 1085-1088.
9. W. L. Barnes, A. Dereux and T. W. Ebbesen, *Nature*, 2003, **424**, 824-830.
10. J. R. Adleman, D. A. Boyd, D. G. Goodwin and D. Psaltis, *Nano Lett.*, 2009, **9**, 4417-4423.
11. J. Christensen, A. Manjavacas, S. Thongrattanasiri, F. H. L. Koppens and F. J. García de Abajo, *ACS Nano*, 2011, **6**, 431-440.
12. W. Gao, J. Shu, C. Qiu and Q. Xu, *ACS Nano*, 2012, **6**, 7806-7813.
13. F. Bonaccorso, Z. Sun, T. Hasan and A. C. Ferrari, *Nat. Photonics*, 2010, **4**, 611-622.
14. Q. Bao and K. P. Loh, *ACS Nano*, 2012, **6**, 3677-3694.
15. A. V. Gorbach, *Phys. Rev. A*, 2013, **87**, 013830.
16. A. N. Grigorenko, M. Polini and K. S. Novoselov, *Nat. Photonics*, 2012, **6**, 749-758.
17. M. Jablan, H. Buljan and M. Soljačić, *Phys. Rev. B*, 2009, **80**, 245435.
18. L. Ju, B. Geng, J. Horng, C. Girit, M. Martin, Z. Hao, H. A. Bechtel, X. Liang, A. Zettl, Y. R. Shen and F. Wang, *Nat. Nanotechnol.*, 2011, **6**, 630-634.

19. F. H. L. Koppens, D. E. Chang and F. J. García de Abajo, *Nano Lett.*, 2011, **11**, 3370-3377.
20. W. B. Lu, W. Zhu, H. J. Xu, Z. H. Ni, Z. G. Dong and T. J. Cui, *Opt. Express*, 2013, **21**, 10475-10482.
21. S. A. Maier, *Nat. Phys.*, 2012, **8**, 581-582.
22. L. Rast, T. J. Sullivan and V. K. Tewary, *Phys. Rev. B*, 2013, **87**, 045428.
23. P. Tassin, T. Koschny, M. Kafesaki and C. M. Soukoulis, *Nat. Photonics*, 2012, **6**, 259-264.
24. T. Low and P. Avouris, *ACS Nano*, 2014, **8**, 1086-1101.
25. A. A. Balandin, S. Ghosh, W. Bao, I. Calizo, D. Teweldebrhan, F. Miao and C. N. Lau, *Nano Lett.*, 2008, **8**, 902-907.
26. A. Roberts, D. Cormode, C. Reynolds, T. Newhouse-Illige, B. J. LeRoy and A. S. Sandhu, *Appl. Phys. Lett.*, 2011, **99**, 051912-051912-051913.
27. E. Hendry, P. J. Hale, J. Moger, A. K. Savchenko and S. A. Mikhailov, *Phys. Rev. Lett.*, 2010, **105**, 097401.
28. S. Thongrattanasiri, F. H. L. Koppens and F. J. García de Abajo, *Phys. Rev. Lett.*, 2012, **108**, 047401.
29. L. Wu, H. S. Chu, W. S. Koh and E. P. Li, *Opt. Express*, 2010, **18**, 14395-14400.
30. A. Vakil and N. Engheta, *Science*, 2011, **332**, 1291-1294.
31. J. T. Kim and S.-Y. Choi, *Opt. Express*, 2011, **19**, 24557-24562.
32. F. Xia, T. Mueller, Y. M. Lin, A. Valdes-Garcia and P. Avouris, *Nat. Nanotechnol.*, 2009, **4**, 839-843.
33. N. Papasimakis, Z. Luo, Z. X. Shen, F. De Angelis, E. Di Fabrizio, A. E. Nikolaenko and N. I. Zheludev, *Opt. Express*, 2010, **18**, 8353-8359.
34. V. G. Kravets, F. Schedin, R. Jalil, L. Britnell, K. S. Novoselov and A. N. Grigorenko, *J. Phys. Chem. C*, 2012, **116**, 3882-3887.
35. F. Xia, V. Perebeinos, Y.-M. Lin, Y. Wu and P. Avouris, *Nat. Nanotechnol.*, 2011, **6**, 179-184.
36. A. Politano and G. Chiarello, *Appl. Phys. Lett.*, 2013, **102**, 201608-201604.
37. A. Politano and G. Chiarello, *Nanoscale*, 2013, **5**, 8215-8220.
38. G. Giovannetti, P. A. Khomyakov, G. Brocks, V. M. Karpan, J. van den Brink and P. J. Kelly, *Phys. Rev. Lett.*, 2008, **101**, 026803.
39. C. Gong, D. Hinojos, W. Wang, N. Nijem, B. Shan, R. M. Wallace, K. Cho and Y. J. Chabal, *ACS Nano*, 2012, **6**, 5381-5387.
40. K. L. Grosse, M.-H. Bae, F. Lian, E. Pop and W. P. King, *Nat. Nanotechnol.*, 2011, **6**, 287-290.
41. C. Gong, S. McDonnell, X. Qin, A. Azcatl, H. Dong, Y. J. Chabal, K. Cho and R. M. Wallace, *ACS Nano*, 2013, **8**, 642-649.
42. J. T. Smith, A. D. Franklin, D. B. Farmer and C. D. Dimitrakopoulos, *ACS Nano*, 2013, **7**, 3661-3667.
43. C. Archambault and A. Rochefort, *ACS Nano*, 2013, **7**, 5414-5420.
44. P. Janthon, F. Vines, S. M. Kozlov, J. Limtrakul and F. Illas, *J. Chem. Phys.*, 2013, **138**, 244701-244708.
45. F. Menges, H. Riel, A. Stemmer, C. Dimitrakopoulos and B. Gotsmann, *Phys. Rev. Lett.*, 2013, **111**, 205901.
46. O. Salihoglu, S. Balci and C. Kocabas, *Appl. Phys. Lett.*, 2012, **100**, 213110-213115.
47. N. Reckinger, A. Vlad, S. Melinte, J.-F. Colomer and M. Sarrazin, *Appl. Phys. Lett.*, 2013, **102**, 211108-211108-211104.
48. P. Zuppella, S. Tosatto, A. J. Corso, S. Zuccon and M. G. Pelizzo, *J. Opt.*, 2013, **15**, 055010.
49. P. Burset, A. L. Yeyati and A. Martín-Rodero, *Phys. Rev. B*, 2008, **77**, 205425.
50. H. B. Heersche, P. Jarillo-Herrero, J. B. Oostinga, L. M. K. Vandersypen and A. F. Morpurgo, *Nature*, 2007, **446**, 56-59.
51. C. Ojeda-Aristizabal, M. Ferrier, S. Guéron and H. Bouchiat, *Phys. Rev. B*, 2009, **79**, 165436.
52. M. Weser, Y. Rehder, K. Horn, M. Sicot, M. Fonin, A. B. Preobrajenski, E. N. Voloshina, E. Goering and Y. S. Dedkov, *Appl. Phys. Lett.*, 2010, **96**, 012504.
53. M. Sepioni, R. R. Nair, S. Rablen, J. Narayanan, F. Tuna, R. Winpenny, A. K. Geim and I. V. Grigorieva, *Phys. Rev. Lett.*, 2010, **105**, 207205.
54. E. J. G. Santos, S. Riikonen, D. Sánchez-Portal and A. Ayuela, *J. Phys. Chem. C*, 2012, **116**, 7602-7606.
55. M. Suzuki, I. S. Suzuki and J. Walter, *Phys. Rev. B*, 2003, **67**, 944061-9440611.
56. H. Yang, J. Heo, S. Park, H. J. Song, D. H. Seo, K.-E. Byun, P. Kim, I. Yoo, H.-J. Chung and K. Kim, *Science*, 2012, **336**, 1140-1143.
57. D. Jiménez, *Nanotechnology*, 2008, **19**, 345204.
58. X. Wu, M. Sprinkle, X. Li, F. Ming, C. Berger and W. A. de Heer, *Phys. Rev. Lett.*, 2008, **101**, 026801.
59. M. Rocca, *Surf. Sci. Rep.*, 1995, **22**, 1-71.
60. A. Politano, G. Chiarello, G. Benedek, E. V. Chulkov and P. M. Echenique, *Surf. Sci. Rep.*, 2013, **68**, 305-389.
61. T. Eberlein, U. Bangert, R. R. Nair, R. Jones, M. Gass, A. L. Bleloch, K. S. Novoselov, A. Geim and P. R. Briddon, *Phys. Rev. B*, 2008, **77**, 233406.
62. P. E. Trevisanutto, C. Giorgetti, L. Reining, M. Ladisa and V. Olevano, *Phys. Rev. Lett.*, 2008, **101**, 226405.

63. N. Ju, A. Bulgac and J. W. Keller, *Phys. Rev. B*, 1993, **48**, 9071-9079.
64. L. Henrard, F. Malengreau, P. Rudolf, K. Hevesi, R. Caudano, P. Lambin and T. Cabioch, *Phys. Rev. B*, 1999, **59**, 5832-5836.
65. G. Chiarello, E. Maccallini, R. G. Agostino, T. Caruso, V. Formoso, L. Papagno, E. Colavita, A. Goldoni, R. Larciprete, S. Lizzit and L. Petaccia, *Phys. Rev. B*, 2004, **69**, 153409.
66. S. Segui, Z. L. Mišković, J. L. Gervasoni and N. R. Arista, *J. Phys.: Condens. Matter*, 2013, **25**, 175001.
67. M. H. Upton, R. F. Klie, J. P. Hill, T. Gog, D. Casa, W. Ku, Y. Zhu, M. Y. Sfeir, J. Misewich, G. Eres and D. Lowndes, *Carbon*, 2009, **47**, 162-168.
68. G. Chiarello, E. Maccallini, R. G. Agostino, V. Formoso, A. Cupolillo, D. Pacilé, E. Colavita, L. Papagno, L. Petaccia, R. Larciprete, S. Lizzit and A. Goldoni, *Carbon*, 2003, **41**, 985-992.
69. A. G. Marinopoulos, L. Reining, A. Rubio and V. Olevano, *Phys. Rev. B*, 2004, **69**, 245419.
70. C. Kramberger, R. Hambach, C. Giorgetti, M. H. Rummeli, M. Knupfer, J. Fink, B. Büchner, L. Reining, E. Einarsson, S. Maruyama, F. Sottile, K. Hannewald, V. Olevano, A. G. Marinopoulos and T. Pichler, *Phys. Rev. Lett.*, 2008, **100**, 196803.
71. A. Politano, A. R. Marino, V. Formoso, D. Farías, R. Miranda and G. Chiarello, *Plasmonics*, 2012, **7**, 369-376.
72. J. Lu, K. P. Loh, H. Huang, W. Chen and A. T. S. Wee, *Phys. Rev. B*, 2009, **80**, 113410.
73. M. K. Kinyanjui, C. Kramberger, T. Pichler, J. C. Meyer, P. Wachsmuth, G. Benner and U. Kaiser, *Europhys. Lett.*, 2012, **97**, 57005.
74. N. Papageorgiou, M. Portail and J. M. Layet, *Surf. Sci.*, 2000, **454-456**, 462-466.
75. X. Liu, T. Pichler, M. Knupfer, M. S. Golden, J. Fink, D. A. Walters, M. J. Casavant, J. Schmidt and R. E. Smalley, *Synth. Met.*, 2001, **121**, 1183-1186.
76. S. Yuan, R. Roldán and M. I. Katsnelson, *Phys. Rev. B*, 2011, **84**, 035439.
77. U. Diebold, A. Preisinger, P. Schattschneider and P. Varga, *Surf. Sci.*, 1988, **197**, 430-443.
78. U. Büchner, *Phys. Status Solidi B*, 1977, **81**, 227-234.
79. K. Zeppenfeld, *Opt. Commun.*, 1969, **1**, 119-122.
80. R. Rosei, S. Modesti, F. Sette, C. Quaresima, A. Savoia and P. Perfetti, *Phys. Rev. B*, 1984, **29**, 3416-3422.
81. A. V. Generalov and Y. S. Dedkov, *Carbon*, 2012, **50**, 183-191.
82. K. V. Emtsev, F. Speck, T. Seyller, L. Ley and J. D. Riley, *Phys. Rev. B*, 2008, **77**, 155303.
83. T. Ohta, A. Bostwick, J. L. McChesney, T. Seyller, K. Horn and E. Rotenberg, *Phys. Rev. Lett.*, 2007, **98**.
84. P. Sutter, J. T. Sadowski and E. Sutter, *Phys. Rev. B*, 2009, **80**, 245411.
85. F. Mittendorfer, A. Garhofer, J. Redinger, J. Klimeš, J. Harl and G. Kresse, *Phys. Rev. B*, 2011, **84**, 201401.
86. D. Pines, *Elementary Excitations in Solids*, Benjamin, New York, 1964.
87. A. Cupolillo, N. Ligato and L. S. Caputi, *Carbon*, 2012, **50**, 2588-2591.
88. G. Gómez-Santos and T. Stauber, *Europhys. Lett.*, 2012, **99**, 27006.
89. S. Thongrattanasiri, I. Silveiro and F. Javier Garcia de Abajo, *Appl. Phys. Lett.*, 2012, **100**, 201105-201105-201104.
90. L. A. Falkovsky, *J. Exp. Theor. Phys.*, 2008, **106**, 575-580.
91. B. Diaconescu, K. Pohl, L. Vattuone, L. Savio, P. Hofmann, V. M. Silkin, J. M. Pitarke, E. V. Chulkov, P. M. Echenique, D. Farías and M. Rocca, *Nature*, 2007, **448**, 57-59.
92. V. Despoja, K. Dekanić, M. Šunjić and L. Marušić, *Phys. Rev. B*, 2012, **86**, 165419.
93. V. Despoja, D. Novko, K. Dekanić, M. Šunjić and L. Marušić, *Phys. Rev. B*, 2013, **87**, 075447.
94. Y. Gao, Z. Yuan and S. Gao, *J. Chem. Phys.*, 2011, **134**, 134702.
95. Z. Yuan and S. Gao, *Surf. Sci.*, 2008, **602**, 460-464.
96. S. J. Allen, D. C. Tsui and R. A. Logan, *Phys. Rev. Lett.*, 1977, **38**, 980.
97. T. Inaoka, T. Nagao, S. Hasegawa, T. Hildebrandt and M. Henzler, *Phys. Rev. B*, 2002, **66**, 2453201-2453208.
98. T. Nagao, T. Hildebrandt, M. Henzler and S. Hasegawa, *Surf. Sci.*, 2001, **493**, 680-686.
99. T. Angot and G. Gewinner, *J. Electron Spectrosc. Relat. Phenom.*, 1999, **104**, 173-184.
100. F. Varchon, R. Feng, J. Hass, X. Li, B. N. Nguyen, C. Naud, P. Mallet, J. Y. Veillen, C. Berger, E. H. Conrad and L. Magaud, *Phys. Rev. Lett.*, 2007, **99**, 126805.
101. X. Luo, T. Qiu, W. Lu and Z. Ni, *Mater. Sci. Eng., R*, 2013, **74**, 351-376.
102. K. Kechedzhi, V. I. Fal'ko, E. McCann and B. L. Altshuler, *Phys. Rev. Lett.*, 2007, **98**, 176806.
103. M. Koshino and E. McCann, *Phys. Rev. B*, 2009, **80**, 165409.
104. B. N. Narozhny, *Phys. Rev. B*, 2007, **76**, 153409.
105. J. M. Pereira, F. M. Peeters, R. N. Costa Filho and G. A. Farias, *J. Phys.: Condens. Matter*, 2009, **21**, 045301.
106. P. Rakyta, A. Kormányos and J. Cserti, *Phys. Rev. B*, 2010, **82**, 113405.
107. A. Politano, A. R. Marino and G. Chiarello, *Phys. Rev. B*, 2012, **86**, 085420.
108. A. Politano, A. R. Marino, V. Formoso, D. Farías, R. Miranda and G. Chiarello, *Phys. Rev. B*, 2011, **84**, 033401.

109. A. Politano, V. Formoso and G. Chiarello, *J. Phys.: Condens. Matter*, 2013, **25**, 345303.
110. T. Langer, D. F. Förster, C. Busse, T. Michely, H. Pfnür and C. Tegenkamp, *New J. Phys.*, 2011, **13**, 053006.
111. V. M. Silkin, A. Garcia-Lekue, J. M. Pitarke, E. V. Chulkov, E. Zaremba and P. M. Echenique, *Europhys. Lett.*, 2004, **66**, 260-264.
112. V. M. Silkin, J. M. Pitarke, E. V. Chulkov and P. M. Echenique, *Phys. Rev. B*, 2005, **72**, 115435.
113. N. J. M. Horing, *Philos. Trans. R. Soc. A*, 2010, **368**, 5525-5556.
114. M. van Schilfgaarde and M. I. Katsnelson, *Phys. Rev. B*, 2011, **83**, 081409.
115. A. Cupolillo, N. Ligato and L. Caputi, *Surf. Sci.*, 2013, **608**, 88-91.
116. Y. Gao and Z. Yuan, *Solid State Commun.*, 2011, **151**, 1009-1013.
117. F. M. D. Pellegrino, G. G. N. Angilella and R. Pucci, *Phys. Rev. B*, 2010, **82**, 115434.
118. A. Politano and G. Chiarello, *Carbon*, 2014, **71**, 176-180.
119. T. Stauber and G. Gómez-Santos, *Phys. Rev. B*, 2012, **85**, 075410.
120. X.-F. Wang and T. Chakraborty, *Phys. Rev. B*, 2007, **75**, 041404.
121. R. Roldán and L. Brey, *Phys. Rev. B*, 2013, **88**, 115420.
122. R. Sensarma, E. H. Hwang and S. Das Sarma, *Phys. Rev. B*, 2010, **82**, 195428.
123. C. Triola and E. Rossi, *Phys. Rev. B*, 2012, **86**, 161408.
124. H. Yu and J. C. Hermanson, *Phys. Rev. B*, 1989, **40**, 11851.
125. E. H. Hwang and S. Das Sarma, *Phys. Rev. B*, 2007, **75**, 205418.
126. Z. Fang, Y. Wang, Z. Liu, A. Schlather, P. M. Ajayan, F. H. L. Koppens, P. Nordlander and N. J. Halas, *ACS Nano*, 2012, **6**, 10222-10228.
127. H. Yan, X. Li, B. Chandra, G. Tulevski, Y. Wu, M. Freitag, W. Zhu, P. Avouris and F. Xia, *Nat Nano*, 2012, **7**, 330-334.
128. S. Y. Shin, N. D. Kim, J. G. Kim, K. S. Kim, D. Y. Noh and J. W. Chung, *Appl. Phys. Lett.*, 2011, **99**, 082110.
129. C. Tegenkamp, H. Pfnür, T. Langer, J. Baringhaus and H. W. Schumacher, *J. Phys.: Condens. Matter*, 2011, **23**, 012001.
130. A. Cupolillo, N. Ligato and L. S. Caputi, *Appl. Phys. Lett.*, 2013, **102**, 111609-111604.
131. G. Bertoni, L. Calmels, A. Altibelli and V. Serin, *Phys. Rev. B*, 2005, **71**, 075402.
132. M. Hasegawa, K. Nishidate, T. Hosokai and N. Yoshimoto, *Phys. Rev. B*, 2013, **87**, 085439.
133. D. Farías, A. M. Shikin, K. H. Rieder and Y. S. Dedkov, *J. Phys.: Cond. Matt.*, 1999, **11**, 8453-8458.
134. A. M. Shikin, D. Farías, V. K. Adamchuk and K. H. Rieder, *Surf. Sci.*, 1999, **424**, 155-167.
135. N. Ligato, A. Cupolillo and L. S. Caputi, *Thin Solid Films*, 2013, **543**, 59-62.
136. Y. Yang, K. Brenner and R. Murali, *Carbon*, 2012, **50**, 1727-1733.
137. X. Feng, S. Maier and M. Salmeron, *J. Am. Chem. Soc.*, 2012, **134**, 5662-5668.
138. P. L. Levesque, S. S. Sabri, C. M. Aguirre, J. Guillemette, M. Siaj, P. Desjardins, T. Szkopek and R. Martel, *Nano Lett.*, 2010, **11**, 132-137.
139. H. Pinto, R. Jones, J. P. Goss and P. R. Briddon, *Phys. Status Solidi A*, 2010, **207**, 2131-2136.
140. A. Politano and G. Chiarello, *Carbon*, 2013, **62**, 263-269.
141. A. Politano and G. Chiarello, *Carbon*, 2013, **61**, 412-417.
142. A. Politano, A. R. Marino, V. Formoso and G. Chiarello, *AIP Advances*, 2011, **1**, 042130.
143. J. S. Qi, J. Y. Huang, J. Feng, D. N. Shi and J. Li, *ACS Nano*, 2011, **5**, 3475-3482.
144. R. Balog, B. Jørgensen, L. Nilsson, M. Andersen, E. Rienks, M. Bianchi, M. Fanetti, E. Lægsgaard, A. Baraldi, S. Lizzit, Z. Slijivancanin, F. Besenbacher, B. Hammer, T. G. Pedersen, P. Hofmann and L. Hornekær, *Nat. Mater.*, 2010, **9**, 315-319.
145. D. Haberer, D. V. Vyalikh, S. Taioli, B. Dora, M. Farjam, J. Fink, D. Marchenko, T. Pichler, K. Ziegler, S. Simonucci, M. S. Dresselhaus, M. Knupfer, B. Büchner and A. Grüneis, *Nano Lett.*, 2010, **10**, 3360-3366.
146. S. Rajasekaran, S. Kaya, F. Abild-Pedersen, T. Anniyev, F. Yang, D. Stacchiola, H. Ogasawara and A. Nilsson, *Phys. Rev. B*, 2012, **86**, 075417.
147. A. Politano, D. Campi, V. Formoso and G. Chiarello, *Phys. Chem. Chem. Phys.*, 2013, **15**, 11356-11361.
148. B. Borca, S. Barja, M. Garnica, M. Minniti, A. Politano, J. M. Rodríguez-García, J. J. Hinarejos, D. Farías, A. L. Vázquez de Parga and R. Miranda, *New J. Phys.*, 2010, **12**, 093018.
149. M. Gyamfi, T. Eelbo, M. Waśniowska and R. Wiesendanger, *Phys. Rev. B*, 2011, **83**, 153418.
150. W. Feng, S. Lei, Q. Li and A. Zhao, *J. Phys. Chem. C*, 2011, **115**, 24858-24864.
151. S. Marchini, S. Günther and J. Wintterlin, *Phys. Rev. B*, 2007, **76**, 075429.
152. B. Wang, M. L. Bocquet, S. Marchini, S. Günther and J. Wintterlin, *Phys. Chem. Chem. Phys.*, 2008, **10**, 3530-3534.
153. F. Moresco, M. Rocca, T. Hildebrandt and M. Henzler, *Phys. Rev. Lett.*, 1999, **83**, 2238-2241.
154. A. Politano, V. Formoso, E. Colavita and G. Chiarello, *Phys. Rev. B*, 2009, **79**, 045426.

155. A. Politano, V. Formoso and G. Chiarello, *Superlattices Microstruct.*, 2009, **46**, 137-140.
156. A. Politano, B. Borca, M. Minniti, J. J. Hinarejos, A. L. Vázquez de Parga, D. Farías and R. Miranda, *Phys. Rev. B*, 2011, **84**, 035450.
157. T. Langer, J. Baringhaus, H. Pfnür, H. W. Schumacher and C. Tegenkamp, *New J. Phys.*, 2010, **12**, 033017.
158. R. Tediosi, N. P. Armitage, E. Giannini and D. van der Marel, *Phys. Rev. Lett.*, 2007, **99**, 016406.
159. M. Jablan, M. Soljačić and H. Buljan, *Phys. Rev. B*, 2011, **83**, 161409.
160. Y. Liu and R. F. Willis, *Phys. Rev. B*, 2010, **81**, 081406.
161. H. Yan, T. Low, W. Zhu, Y. Wu, M. Freitag, X. Li, F. Guinea, P. Avouris and F. Xia, *Nat. Photonics*, 2013, **7**, 394-399.
162. A. Bostwick, F. Speck, T. Seyller, K. Horn, M. Polini, R. Asgari, A. H. MacDonald and E. Rotenberg, *Science*, 2010, **328**, 999-1002.
163. P. Van-Nham and F. Holger, *New J. Phys.*, 2012, **14**, 075007.
164. J. P. Carbotte, J. P. F. LeBlanc and E. J. Nicol, *Phys. Rev. B*, 2012, **85**, 201411.
165. P. M. Krstajić and F. M. Peeters, *Phys. Rev. B*, 2012, **85**, 205454.
166. P. M. Krstajić and F. M. Peeters, *Phys. Rev. B*, 2013, **88**, 165420.
167. J. P. F. LeBlanc and J. P. Carbotte, *Phys. Rev. B*, 2013, **87**, 205407.
168. A. L. Walter, A. Bostwick, K.-J. Jeon, F. Speck, M. Ostler, T. Seyller, L. Moreschini, Y. J. Chang, M. Polini, R. Asgari, A. H. MacDonald, K. Horn and E. Rotenberg, *Phys. Rev. B*, 2011, **84**, 085410.
169. J. Lischner, D. Vigil-Fowler and S. G. Louie, *Phys. Rev. Lett.*, 2013, **110**, 146801.
170. V. I. Belotelov, I. A. Akimov, PohlM, V. A. Kotov, KastureS, A. S. Vengurlekar, A. V. Gopal, D. R. Yakovlev, A. K. Zvezdin and BayerM, *Nat. Nanotechnol.*, 2011, **6**, 370-376.
171. V. Bonanni, S. Bonetti, T. Pakizeh, Z. Pirzadeh, J. Chen, J. Nogués, P. Vavassori, R. Hillenbrand, J. Åkerman and A. Dmitriev, *Nano Lett.*, 2011, **11**, 5333-5338.
172. Y. E. Lozovik and A. A. Sokolik, *Nanoscale Res. Lett.*, 2012, **7**, 1-19.
173. C. Li and F. Zhai, *J. Appl. Phys.*, 2011, **109**, 093306.
174. M. A. Eriksson, A. Pinczuk, B. S. Dennis, S. H. Simon, L. N. Pfeiffer and K. W. West, *Phys. Rev. Lett.*, 1999, **82**, 2163-2166.
175. S. Cinà, D. M. Whittaker, D. D. Arnone, T. Burke, H. P. Hughes, M. Leadbeater, M. Pepper and D. A. Ritchie, *Phys. Rev. Lett.*, 1999, **83**, 4425-4428.
176. H. C. A. Oji and A. H. MacDonald, *Phys. Rev. B*, 1986, **33**, 3810-3818.
177. Y. A. Bychkov and G. Martinez, *Phys. Rev. B*, 2002, **66**, 193312.
178. C. Kallin and B. I. Halperin, *Phys. Rev. B*, 1984, **30**, 5655-5668.
179. O. L. Berman, G. Gumbs and P. M. Echenique, *Phys. Rev. B*, 2009, **79**, 075418.
180. W. Wang, S. P. Apell and J. M. Kinaret, *Phys. Rev. B*, 2012, **86**, 125450.
181. Y. A. Bychkov and G. Martinez, *Phys. Rev. B*, 2008, **77**, 125417.
182. Y. A. Bychkov and G. Martinez, *Physica E*, 2008, **40**, 1410-1411.
183. N. Chamanara, D. Sounas and C. Caloz, *Opt. Express*, 2013, **21**, 11248-11256.
184. N. Chamanara, D. Sounas, T. Szkopek and C. Caloz, *Opt. Express*, 2013, **21**, 25356-25363.
185. M. Tahir and K. Sabeeh, *Phys. Rev. B*, 2007, **76**, 195416.
186. M. Tahir, K. Sabeeh and A. MacKinnon, *J. Phys.: Condens. Matt.*, 2011, **23**, 425304.
187. V. E. Bisti and N. N. Kirova, *Physica B*, 2012, **407**, 1923-1926.
188. A. Ferreira, N. M. R. Peres and A. H. Castro Neto, *Phys. Rev. B*, 2012, **85**, 205426.
189. A. M. Fischer, A. B. Dzyubenko and R. A. Römer, *Phys. Rev. B*, 2009, **80**, 165410.
190. A. M. Fischer, R. A. Römer and A. B. Dzyubenko, *Europhys. Lett.*, 2010, **92**, 37003.
191. I. Petković, F. I. B. Williams, K. Bennaceur, F. Portier, P. Roche and D. C. Glattli, *Phys. Rev. Lett.*, 2013, **110**, 016801.
192. J. Y. Wu, S. C. Chen, O. Roslyak, G. Gumbs and M. F. Lin, *ACS Nano*, 2011, **5**, 1026-1032.
193. H. Yan, Z. Li, X. Li, W. Zhu, P. Avouris and F. Xia, *Nano Lett.*, 2012, **12**, 3766-3771.
194. O. L. Berman, G. Gumbs and Y. E. Lozovik, *Phys. Rev. B*, 2008, **78**, 085401.
195. R. Roldán, J. N. Fuchs and M. O. Goerbig, *Phys. Rev. B*, 2009, **80**, 085408.
196. I. Crassee, M. Orlita, M. Potemski, A. L. Walter, M. Ostler, T. Seyller, I. Gaponenko, J. Chen and A. B. Kuzmenko, *Nano Lett.*, 2012, **12**, 2470-2474.
197. D. C. Glattli, E. Y. Andrei, G. Deville, J. Poitrenaud and F. I. B. Williams, *Phys. Rev. Lett.*, 1985, **54**, 1710-1713.
198. D. B. Mast, A. J. Dahm and A. L. Fetter, *Phys. Rev. Lett.*, 1985, **54**, 1706-1709.
199. I. V. Kukushkin, J. H. Smet, S. A. Mikhailov, D. V. Kulakovskii, K. von Klitzing and W. Wegscheider, *Phys. Rev. Lett.*, 2003, **90**, 156801.
200. S. J. Allen, H. L. Störmer and J. C. M. Hwang, *Phys. Rev. B*, 1983, **28**, 4875-4877.

201. A. L. Fetter, *Phys. Rev. B*, 1985, **32**, 7676-7684.
202. Z. Fei, A. S. Rodin, G. O. Andreev, W. Bao, A. S. McLeod, M. Wagner, L. M. Zhang, Z. Zhao, M. Thiemens and G. Dominguez, *Nature*, 2012, **487**, 82-85.
203. J. Chen, M. Badioli, P. Alonso-González, S. Thongrattanasiri, F. Huth, J. Osmond, M. Spasenović, A. Centeno, A. Pesquera and P. Godignon, *Nature*, 2012, **487**, 77-81.
204. J. Chen, M. L. Nesterov, A. Y. Nikitin, S. Thongrattanasiri, P. Alonso-González, T. M. Slipchenko, F. Speck, M. Ostler, T. Seyller, I. Crassee, F. H. L. Koppens, L. Martin-Moreno, F. J. García de Abajo, A. B. Kuzmenko and R. Hillenbrand, *Nano Lett.*, 2013, **13**, 6210-6215.
205. A. Manjavacas, P. Nordlander and F. J. García de Abajo, *ACS Nano*, 2012, **6**, 1724-1731.
206. P. Liu, W. Cai, L. Wang, X. Zhang and J. Xu, *Appl. Phys. Lett.*, 2012, **100**, 153111-153111-153115.
207. Y. Wang, E. W. Plummer and K. Kempa, *Adv. Phys.*, 2011, **60**, 799-898.
208. V. Ryzhii, A. A. Dubinov, T. Otsuji, V. Mitin and M. S. Shur, *J. Appl. Phys.*, 2010, **107**, 054505.
209. A. R. Davoyan, M. Y. Morozov, V. V. Popov, A. Satou and T. Otsuji, *Appl. Phys. Lett.*, 2013, **103**, 251102.
210. V. Ryzhii, A. A. Dubinov, T. Otsuji, V. Y. Aleshkin, M. Ryzhii and M. Shur, *Opt. Express*, 2013, **21**, 31567-31577.
211. Z. Fang, Z. Liu, Y. Wang, P. M. Ajayan, P. Nordlander and N. J. Halas, *Nano Lett.*, 2012, **12**, 3808-3813.
212. G. W. Hanson, *J. Appl. Phys.*, 2008, **104**, 084314-084314-084315.
213. P. Liu, X. Zhang, Z. Ma, W. Cai, L. Wang and J. Xu, *Opt. Express*, 2013, **21**, 32432-32440.
214. Y. Shao, J. Wang, H. Wu, J. Liu, I. A. Aksay and Y. Lin, *Electroanalysis*, 2010, **22**, 1027-1036.
215. W. R. Yang, K. R. Ratinac, S. P. Ringer, P. Thordarson, J. J. Gooding and F. Braet, *Angew. Chem.*, 2010, **49**, 2114-2138.
216. U. Stöberl, U. Wurstbauer, W. Wegscheider, D. Weiss and J. Eroms, *Appl. Phys. Lett.*, 2008, **93**, 051906.
217. M. Kauranen and A. V. Zayats, *Nat. Photonics*, 2012, **6**, 737-748.
218. M. Gullans, D. E. Chang, F. H. L. Koppens, F. J. G. de Abajo and M. D. Lukin, *Phys. Rev. Lett.*, 2013, **111**, 247401.
219. P. A. Khomyakov, A. A. Starikov, G. Brocks and P. J. Kelly, *Phys. Rev. B*, 2010, **82**, 115437.